Archive of Applied Mechanics
https://doi.org/10.1007/s00419-024-02613-6

ORIGINAL

Vu Thi Thu Trang · Nguyen Van Long · Tran Minh Tu · Le Thanh Hai

A refined quasi-3D model for buckling and free vibration of functionally graded saturated porous plate resting on elastic foundation

Received: 26 September 2023 / Accepted: 30 April 2024

Abstract This study investigates the buckling and free vibration behavior of functionally graded saturated porous (FGSP) using a refined quasi-3D theory that ensures zero transverse shear stress at the top and bottom surfaces of the plate. The material properties depend on the porosity coefficient according to three patterns. Hamilton's principle and Biot's poroelasticity theory are employed to derive the equations of motion, which are then solved using Navier's technique. After examining the accuracy of the suggested approach, the effect of fluid compressibility on natural frequency and critical buckling load is investigated in the undrained condition. Also, the effect of porosity, geometrical parameters, and elastic foundation on the vibration and buckling response of FGSP plates are examined. The study reveals that saturating the pores with fluid leads to increased plate stiffness. This translates to higher critical buckling loads and fundamental frequencies.

Keywords Buckling response · Vibration analysis · Saturated porous plate · Analytical solution · Quasi-3D theory

1 Introduction

Functionally graded porous materials (FGPM) are ones of advanced lightweight materials, which are created from the idea of combining two different materials, FGMs, and porous materials. The variation of porosity along certain directions causes a continuous change in their mechanical properties. Possess great permeability, resistance to shock, and electrical conductivity, FGPMs have been used in different fields such as aircraft, submarine, energy, sea structures, biophysics, etc. Usually, the pores are filled by the fluid and introduce some specific properties. To study the mechanical behavior of FGP structures, the poroelasticity theory, which was first introduced by Biot [1] is used. Biot's theory includes two conditions: drained and undrained (saturated). In drained conditions, stress–strain relations are expressed as the conventional theory of elasticity (Hooke law).

To analyze the mechanical response of FGP structures, various plate models have been suggested based on particular assumptions. These theories first are developed for isotropic plates, and later improved for composite

V. T. T. Trang
School of Mechanical Engineering, Vietnam Maritime University, 484 Lach Tray Street, Le Chan District, Hai Phong, Viet Nam

N. Van Long (✉) · T. M. Tu
Faculty of Industrial and Civil Engineering, Hanoi University of Civil Engineering (HUCE), 55 Giai Phong Road, Hai Ba Trung District, Ha Noi, Viet Nam
e-mail: longnv@huce.edu.vn

V. T. T. Trang · N. Van Long · T. M. Tu · L. T. Hai
Frontier Research Group of Mechanics of Advanced Materials and Structures (MAMS), HUCE - 55 Giai Phong Road, Hai Ba Trung District, Ha Noi, Viet Nam

L. T. Hai
Vinh University, 182 Le Duan Road, Vinh, Nghe An, Viet Nam

Published online: 13 May 2024

plates. The buckling response and vibrational characteristic of plates are important problems in the design process, thus the studies focused on this topic are always attracted many researchers. There are numerous works published related to the FGP plates in the drained conditions that Hooke law is used to describe the stress–strain relation [2–5]. Recently, research on the dynamic response of FGP plates in undrained conditions (FGSP—functionally graded saturated porous plates) has also received more and more attention.

Based on Kirchhoff's hypothesis, classical plate theory (CPT) is developed by Love. This is the simplest plate theory and is appropriate only for thin plates because of neglecting the shear and normal strains. Theodorakopoulos and Beskos [6] presented a vibration analysis of FGSP rectangular plates including the inertia effects. Leclaire et al. [7] investigated the vibrational characteristics of a thin FGSP plate. Jabbari et al. [8] reported a stability analysis of FGSP circular plates under only compressive radial loading, and taking into account the thermal effect [9, 10]. Later, the buckling behaviour of the FGSP rectangular plate embedded with a piezoelectric actuator is explored by Jabbari et al. [11] by using an analytical approach.

Since CPT does not provide consistent results for thick plates, first-order shear deformation theories (FSDT) are suggested. FSDT assumes that in-plane displacements are linear functions of plate thickness variables and have been used widely because of their simplicity. Rezaei and Saidi [12, 13] predicted critical buckling load and natural frequencies of the FGSP annular sector plate by using an analytical approach. These authors [14] reported the impact of coupled solid–fluid deformation on the free vibrational characteristics of the FGSP rectangular plate under the Levy-type boundary condition. Chen et al. [15] investigated the static and buckling response of an FGP (in drained condition) plate using FSDT and Chebyshev-Ritz method. By employing the improved Fourier series method, Zhao et al. [16] presented the free vibration of the FGP plate under different boundary conditions. Utilizing the GDQM, Khouzestani and Khorshidvand [17] predicted the natural frequencies and stress field of the FGSP annular plate.

Since in-plane displacements of FSDT are supposed to be linearly varied along the plate thickness, it does not reflect the real parabolic change of the shear stress along the plate thickness, therefore it is necessary to include the shear correction factor. However, the exact values of these factors depend on several factors, such as plate geometry**,** boundary conditions**,** and material properties. To overcome the drawbacks of FSDT, various HSDTs are developed. By assuming negligible strains and stresses through the thickness, the 3D elasticity problem of a plate reduces to 2D plate theories. These theories were initially proposed for isotropic and laminated composite plates and then extended to FGM and FGSP plates. For example, Sharifan and Jabbari [18] investigated the stability of the FGSP elliptical plate subjected to in-plane compressive forces. Mojahedin et al. [19] predicted the buckling load of the FGSP circular plate by applying HSDT, and the obtained results are compared with those used CLPT and FSDT. Within the framework of Reddy's HSDT and FSDT, Rad et al. [20] presented an elastic buckling analysis of an FGSP plate with Levy boundary conditions. Using Reddy's HSDT and analytical approach, Rezaei and Saidi [21] predicted the natural frequency of the FGSP plate.

While 3D elasticity theory provides the most general solution, its mathematical complexity makes it computationally expensive and time-consuming. Therefore, this approach is rarely used for FGSP plates, only a few studies have been published. Using the 3D elasticity theory, Kiarasi et al. [22] presented the 3D solution to explore the buckling behavior of rectangular FGSP plates under various loading types by using the FE-GDQ method (combination of FEM and generalized DQM). Using three-dimensional finite element, Babaei et al. presented bending and free vibrational characteristics of FGSP annular elliptical sector plate [23], free vibration, and dynamic response of FGSP annular sector plate and cylindrical panels [24, 25].

Beam, plate, and shell structures on elastic foundations are highly relevant in practical engineering. To understand their mechanical behavior, researchers have proposed and applied various foundation models to analyze both static and dynamic responses of these structures, for instance, Winkler/Pasternak model [26], Winkler/Pasternak/Kerr [27] model, visco-Pasternak model [28–37],

Among the plate theories used in analyzing plate structures, quasi-3D theory is commonly employed. It is favored for its reduced mathematical complexity compared to 3D elasticity theory and its consideration of transverse normal strain and transverse shear strains, which are not accounted for in 2D plate theory. Various quasi-3D theories are used in analyzing FGM plate and shell structures. These theories encompass HSDTs, where the variation in transverse displacement nonlinearly changes across plate thickness and they do not meet the conditions of having vanishing transverse shear stress on both the upper and lower surfaces of the plate [38, 39].

To the best of the authors' knowledge, no comprehensive vibration and buckling analysis has been performed on FGSP plates, representing the novelty of the paper. This study builds upon our previous work [40], which introduced a quasi-3D higher-order shear deformation theory with seven displacement unknowns for static analysis of FGSP plates. This work departs from previous studies by employing Hamilton's principle to

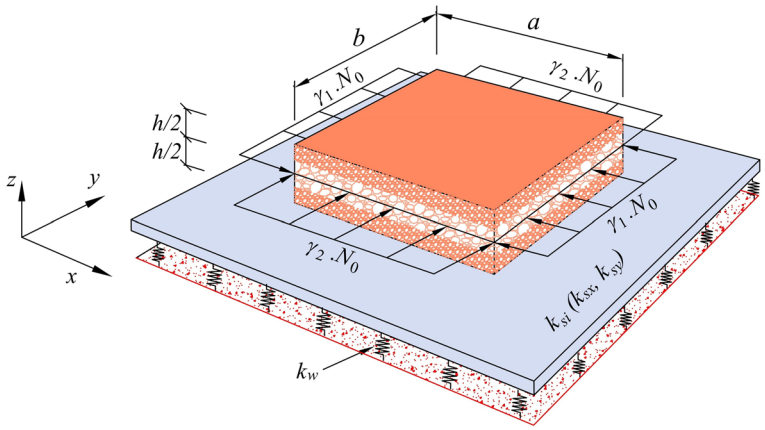

Fig. 1 The configuration of the FGSP plate resting on the Pasternak elastic foundation

derive the governing equations for FGSP plates. Navier's technique is then applied to obtain explicit solutions for natural frequency and critical buckling load. By employing Biot's poroelastic theory, the effect of fluid pressure in the pores on the vibration and buckling response of FGSP plates with three porosity distribution patterns is investigated. Additionally, the influence of porosity coefficient, porosity distribution patterns, plate geometry, and foundation stiffness are examined in detail.

2 Theoretical formulation

2.1 The FGSP plate model

The configuration of an FGSP rectangular plate resting on Pasternak elastic foundation is illustrated in Fig. 1, and the reference coordinate system (x, y, z) located at the mid-plane.

For FGPMs, to determine the effective material properties, different methods have been proposed to link the mesoscopic/microscopic porous geometric features (relative density mainly) with macroscopic material parameters.

Various models have been suggested for FGPMs to establish a connection between the microscopic features of pores (primarily relative density), and the macroscopic material properties to ascertain effective material properties, including the Gibson-Ashby, Christensen, Roberts-Garboczi, Menges-Knipschild, Chen models, and modified rule of mixture [41]. Most of these models were created through experimental or numerical investigations and can be utilized for both open-cell and closed-cell foams by adjusting specific parameters. The relative density is often regarded as the primary determining factor, providing a relatively straightforward method for predicting overall properties. This is achieved by assigning desired distributions of relative density to the structural components. For metal foams, a specific type of foam material, effective material properties are assumed to be changed across plate thickness according to three laws as follows [42, 43]:

- UPD: uniform porosity distribution:

$$\begin{cases} \{E(z), G(z)\} = \{E_{\max}, G_{\max}\}(1 - e_0\psi); \\ \rho(z) = \rho_{\max}\sqrt{1 - e_0\psi}; \\ \psi = \dfrac{1}{e_0} - \dfrac{1}{e_0}\left(\dfrac{2}{\pi}\sqrt{1 - e_0} - \dfrac{2}{\pi} + 1\right)^2 \end{cases} \tag{1}$$

- NUPD-S: non-uniform symmetric porosity distribution [44]:

$$\begin{cases} \{E(z), G(z)\} = \{E_{\max}, G_{\max}\}\left[1 - e_0 \cos\left(\dfrac{\pi z}{h}\right)\right]; \\ \rho(z) = \rho_{\max}\left[1 - e_m \cos\left(\dfrac{\pi z}{h}\right)\right] \end{cases} \tag{2}$$

- NUPD-AS: non-uniform asymmetric porosity distribution [8]:

$$\begin{cases} \{E(z), G(z)\} = \{E_{\max}, G_{\max}\}\left[1 - e_0 \cos\left(\dfrac{\pi z}{2h} + \dfrac{\pi}{4}\right)\right]; \\ \rho(z) = \rho_{\max}\left[1 - e_m \cos\left(\dfrac{\pi z}{2h} + \dfrac{\pi}{4}\right)\right] \end{cases} \tag{3}$$

where $E_{\max}$, $G_{\max}$, $\rho_{\max}$ and $E_{\min}$, $G_{\min}$, $\rho_{\min}$ are extremum values of elastic moduli, and mass density. The Poisson coefficient is assumed to be independent of the thickness coordinate [8, 45]. e_0 is the porosity coefficient ($0 < e_0 < 1$), and is defined by:

$$e_0 = 1 - E_{\min}/E_{\max} = 1 - G_{\min}/G_{\max} \tag{4}$$

The porosity coefficient for mass density e_m ($0 < e_m < 1$) is defined as:

$$e_m = 1 - \rho_{\min}/\rho_{\max} \tag{5}$$

The relation between extremum Young's modulus and mass density for an open-cell metal foam [46, 47], e_0 and e_m [45] is expressed as:

$$\frac{E_{\min}}{E_{\max}} = \left(\frac{\rho_{\min}}{\rho_{\max}}\right)^2; \quad e_m = 1 - \sqrt{1 - e_0} \tag{6}$$

2.2 Displacement field

The refined quasi-3D HSDT used in this study originated from eleven unknown HSDT and also satisfies free transverse shear stresses in the top and bottom surfaces of the plate. The displacement field is given as [40]:

$$\begin{aligned} u_1(x,y,z,t) &= u_1^0(x,y,t) + z\theta_1(x,y,t) - \frac{z^2}{2}\frac{\partial \theta_3}{\partial x} - \frac{z^3}{3}\left[\kappa\left(\frac{\partial u_3^0}{\partial x} + \theta_1\right) + \frac{\partial u_3^*}{\partial x}\right]; \\ u_2(x,y,z,t) &= u_2^0(x,y,t) + z\theta_2(x,y,t) - \frac{z^2}{2}\frac{\partial \theta_3}{\partial y} - \frac{z^3}{3}\left[\kappa\left(\frac{\partial u_3^0}{\partial y} + \theta_2\right) + \frac{\partial u_3^*}{\partial y}\right]; \\ u_3(x,y,z,t) &= u_3^0(x,y,t) + z\theta_3(x,y,t) + z^2 u_3^*(x,y,t) \end{aligned} \tag{7}$$

where $\kappa = \frac{4}{h^2}$; u_1^0, u_2^0, u_3^0 are displacements of a point along (x,y,z) axes, and θ_1, θ_2 are rotations of a transverse normal about the y- and x- axes; θ_3, u_3^* are higher-order terms.

The kinematic relations are expressed as:

$$\begin{aligned} \boldsymbol{\varepsilon} = \begin{Bmatrix} \varepsilon_x \\ \varepsilon_y \\ \varepsilon_z \\ \gamma_{xy} \end{Bmatrix} &= \begin{Bmatrix} \varepsilon_x^0 \\ \varepsilon_y^0 \\ \varepsilon_z^0 \\ \gamma_{xy}^0 \end{Bmatrix} + z\begin{Bmatrix} \varepsilon_x^{(1)} \\ \varepsilon_y^{(1)} \\ \varepsilon_z^{(1)} \\ \gamma_{xy}^{(1)} \end{Bmatrix} + z^2\begin{Bmatrix} \varepsilon_x^{(2)} \\ \varepsilon_y^{(2)} \\ 0 \\ \gamma_{xy}^{(2)} \end{Bmatrix} + z^3\begin{Bmatrix} \varepsilon_x^{(3)} \\ \varepsilon_y^{(3)} \\ 0 \\ \gamma_{xy}^{(3)} \end{Bmatrix}; \\ \boldsymbol{\gamma} = \begin{Bmatrix} \gamma_{xz} \\ \gamma_{yz} \end{Bmatrix} &= \left(1 - \kappa z^2\right)\begin{Bmatrix} \gamma_{xz}^0 \\ \gamma_{yz}^0 \end{Bmatrix} \end{aligned} \tag{8}$$

where

$$\begin{gathered}
\varepsilon_x^0 = \frac{\partial u_1^0}{\partial x}; \quad \varepsilon_x^{(1)} = \frac{\partial \theta_1}{\partial x}; \quad \varepsilon_x^{(2)} = -\frac{1}{2}\frac{\partial^2 \theta_3}{\partial x^2}; \quad \varepsilon_x^{(3)} = -\frac{1}{3}\left[\kappa\left(\frac{\partial^2 u_3^0}{\partial x^2} + \frac{\partial \theta_1}{\partial x}\right) + \frac{\partial u_3^*}{\partial x^2}\right]; \\
\varepsilon_y^0 = \frac{\partial u_2^0}{\partial y}; \quad \varepsilon_y^{(1)} = \frac{\partial \theta_2}{\partial y}; \quad \varepsilon_y^{(2)} = -\frac{1}{2}\frac{\partial^2 \theta_3}{\partial y^2}; \quad \varepsilon_y^{(3)} = -\frac{1}{3}\left[\kappa\left(\frac{\partial^2 u_3^0}{\partial y^2} + \frac{\partial \theta_2}{\partial y}\right) + \frac{\partial u_3^*}{\partial y^2}\right]; \\
\varepsilon_z^0 = \theta_1; \quad \varepsilon_z^{(1)} = 2u_3^*; \quad \gamma_{xy}^0 = \frac{\partial u_1^0}{\partial y} + \frac{\partial u_2^0}{\partial x}; \quad \gamma_{xy}^{(1)} = \left(\frac{\partial \theta_1}{\partial y} + \frac{\partial \theta_2}{\partial x}\right); \\
\gamma_{xy}^{(2)} = -\frac{\partial^2 \theta_3}{\partial x \partial y}; \quad \gamma_{xy}^{(3)} = -\frac{1}{3}\left[\kappa\left(2\frac{\partial^2 u_3^0}{\partial x \partial y} + \frac{\partial \theta_1}{\partial y} + \frac{\partial \theta_2}{\partial x}\right) + 2\frac{\partial^2 u_3^*}{\partial x \partial y}\right]; \\
\gamma_{xz}^0 = \theta_1 + \frac{\partial u_3^0}{\partial x}; \quad \gamma_{yz}^0 = \theta_2 + \frac{\partial u_3^0}{\partial y}
\end{gathered} \tag{9}$$

2.3 Constitutive relations

Based on Biot's poroelasticity theory, stress–strain relations for FSGP plate are given as follows [48]:

$$\begin{gathered}
\sigma_i = 2G\varepsilon_i + \lambda_u \theta - p\alpha_0; \quad i = x, y, z \\
\tau_j = G\gamma_j; \quad j = xy, yz, xz
\end{gathered} \tag{10}$$

where p, α_0, and θ are pore fluid pressure, Biot coefficient of effective stress, and volumetric strain that are defined as:

$$\begin{gathered}
p = M(\xi - \alpha_0 \theta); \quad \alpha_0 = 1 - \frac{G}{G_1}; \quad \theta = \varepsilon_x + \varepsilon_y + \varepsilon_z; \\
M = \frac{2G(\nu_u - \nu)}{\alpha_0^2(1 - 2\nu_u)(1 - 2\nu)}; \quad \lambda_u = \frac{2\nu_u}{1 - 2\nu_u}G; \quad \nu_u = \frac{\nu + \alpha_0 B(1 - 2\nu)/3}{1 - \alpha_0 B(1 - 2\nu)/3}
\end{gathered} \tag{11}$$

in Eq. (9): M is Biot modulus, ν_u is undrained Poisson ratio, ξ is the variation of the fluid volume content, and B is Skempton pore pressure coefficient.

Applying the Biot's theory, the stress–strain relation for FSGP plates can be expressed as:

$$\begin{gathered}
\boldsymbol{\sigma} = \begin{Bmatrix} \sigma_x \\ \sigma_y \\ \sigma_z \\ \tau_{xy} \end{Bmatrix} = G(z) \begin{bmatrix} k_1 & k_2 & k_2 & 0 \\ k_2 & k_1 & k_2 & 0 \\ k_2 & k_2 & k_1 & 0 \\ 0 & 0 & 0 & k_3 \end{bmatrix} \begin{Bmatrix} \varepsilon_x \\ \varepsilon_y \\ \varepsilon_z \\ \gamma_{xy} \end{Bmatrix}; \\
\boldsymbol{\tau} = \begin{Bmatrix} \tau_{xz} \\ \tau_{yz} \end{Bmatrix} = G(z) \begin{bmatrix} 1 & 0 \\ 0 & 1 \end{bmatrix} \begin{Bmatrix} \gamma_{xz} \\ \gamma_{yz} \end{Bmatrix}
\end{gathered} \tag{12}$$

where $k_1 = \frac{2(2\nu_u\nu - 3\nu + 1)}{1 - 2\nu_u - 2\nu + 4\nu\nu_u}; k_2 = \frac{2(2\nu_u - 2\nu_u\nu - \nu)}{1 - 2\nu_u - 2\nu + 4\nu\nu_u}; k_3 = 1.$

Stress resultants are defined as:

$$\begin{gathered}
\begin{bmatrix} N_x & M_x \\ N_y & M_y \\ N_z & M_z \\ N_{xy} & M_{xy} \end{bmatrix} = \int_{-h/2}^{h/2} \begin{Bmatrix} \sigma_x \\ \sigma_y \\ \sigma_z \\ \tau_{xy} \end{Bmatrix} \{ 1 \; z \} dz; \begin{bmatrix} N_x^* & M_x^* \\ N_y^* & M_y^* \\ N_{xy}^* & M_{xy}^* \end{bmatrix} = \int_{-h/2}^{h/2} \begin{Bmatrix} \sigma_x \\ \sigma_y \\ \tau_{xy} \end{Bmatrix} \{ z^2 \; z^3 \} dz; \\
\begin{Bmatrix} R_x \\ R_y \end{Bmatrix} = \int_{-h/2}^{h/2} \begin{Bmatrix} \tau_{xz} \\ \tau_{yz} \end{Bmatrix} \left(1 - \kappa z^2\right) dz
\end{gathered} \tag{13}$$

From Eqs. (8), (12), and (13), the stress resultants can be rewritten in the form:

$$\begin{Bmatrix} N_x \\ N_y \\ N_z \\ N_{xy} \\ M_x \\ M_y \\ M_z \\ M_{xy} \\ N_x^* \\ N_y^* \\ N_{xy}^* \\ M_x^* \\ M_y^* \\ M_{xy}^* \end{Bmatrix} = \begin{bmatrix} A_1 & A_2 & A_2 & 0 & B_1 & B_2 & B_2 & 0 & C_1 & C_2 & 0 & D_1 & D_2 & 0 \\ A_2 & A_1 & A_2 & 0 & B_2 & B_1 & B_2 & 0 & C_2 & C_1 & 0 & D_2 & D_1 & 0 \\ A_2 & A_2 & A_1 & 0 & B_2 & B_2 & B_1 & 0 & C_2 & C_2 & 0 & D_2 & D_2 & 0 \\ 0 & 0 & 0 & A_3 & 0 & 0 & 0 & B_3 & 0 & 0 & C_3 & 0 & 0 & D_3 \\ B_1 & B_2 & B_2 & 0 & C_1 & C_2 & C_2 & 0 & D_1 & D_2 & 0 & E_1 & E_2 & 0 \\ B_2 & B_1 & B_2 & 0 & C_2 & C_1 & C_2 & 0 & D_2 & D_1 & 0 & E_2 & E_1 & 0 \\ B_2 & B_2 & B_1 & 0 & C_2 & C_2 & C_1 & 0 & D_2 & D_2 & 0 & E_2 & E_2 & 0 \\ 0 & 0 & 0 & B_3 & 0 & 0 & 0 & C_3 & 0 & 0 & D_3 & 0 & 0 & E_3 \\ C_1 & C_2 & C_2 & 0 & D_1 & D_2 & D_2 & 0 & E_1 & E_2 & 0 & F_1 & F_2 & 0 \\ C_2 & C_1 & C_2 & 0 & D_2 & D_1 & D_2 & 0 & E_2 & E_1 & 0 & F_2 & F_1 & 0 \\ 0 & 0 & 0 & C_3 & 0 & 0 & 0 & D_3 & 0 & 0 & E_3 & 0 & 0 & F_3 \\ D_1 & D_2 & D_2 & 0 & E_1 & E_2 & E_2 & 0 & F_1 & F_2 & 0 & G_1 & G_2 & 0 \\ D_2 & D_1 & D_2 & 0 & E_2 & E_1 & E_2 & 0 & F_2 & F_1 & 0 & G_2 & G_1 & 0 \\ 0 & 0 & 0 & D_3 & 0 & 0 & 0 & E_3 & 0 & 0 & F_3 & 0 & 0 & G_3 \end{bmatrix} \begin{Bmatrix} \varepsilon_x^0 \\ \varepsilon_y^0 \\ \varepsilon_z^0 \\ \gamma_{xy}^0 \\ \varepsilon_x^{(1)} \\ \varepsilon_y^{(1)} \\ \varepsilon_z^{(1)} \\ \gamma_{xy}^{(1)} \\ \varepsilon_x^{(2)} \\ \varepsilon_y^{(2)} \\ \gamma_{xy}^{(2)} \\ \varepsilon_x^{(2)} \\ \varepsilon_y^{(2)} \\ \gamma_{xy}^{(3)} \end{Bmatrix};$$

$$\begin{Bmatrix} R_x \\ R_y \end{Bmatrix} = \begin{bmatrix} A^s & 0 \\ 0 & A^s \end{bmatrix} \begin{Bmatrix} \gamma_{xz}^0 \\ \gamma_{yz}^0 \end{Bmatrix} \tag{14}$$

where

$$(A_i, B_i, C_i, D_i, E_i, F_i, G_i) = \int_{-h/2}^{h/2} k_i G(z)\left(1, z, z^2, z^3, z^4, z^5, z^6\right) dz; \quad i = 1, 2, 3;$$

$$A^s = \int_{-h/2}^{h/2} G(z)\left(1 - \kappa z^2\right)^2 dz = A_3 - 2\kappa C_3 + \kappa^2 E_3 \tag{15}$$

2.4 Equations of motion

The governing equations of the FGSP plate are derived by using Hamilton's principle [49] and are performed in the variational form:

$$0 = \int_0^T (\delta U_P + \delta U_F + \delta V - \delta K) dt \tag{16}$$

where δU_P is the virtual strain energy, δU_F is the virtual strain energy of the foundation, δV is the virtual work done by external forces, and δK is the virtual kinetic energy.

The virtual strain energy is determined by:

$$\delta U_P = \int_A \int_{-h/2}^{h/2} \left(\boldsymbol{\sigma}^T \delta \boldsymbol{\varepsilon} + \boldsymbol{\tau}^T \delta \boldsymbol{\gamma}\right) dA dz \tag{17}$$

The virtual strain energy of the foundation can be expressed as:

$$\delta U_F = -\int_A f_e^- \delta u_3^- dA = -\int_A f_e^- \left(\delta u_3^0 - \frac{h}{2}\delta\theta_3 + \frac{h^2}{4}\delta u_3^*\right) dA \tag{18}$$

where f_e^- is the reaction of the Pasternak foundation [50]:

$$f_e^- = \left(-k_w u_3 + k_{sx}\frac{\partial^2 u_3}{\partial x^2} + k_{sy}\frac{\partial^2 u_3}{\partial y^2}\right)\Big|_{z=-h/2} \tag{19}$$

The virtual work done by external in-plane forces is given by [51]:

$$\delta V = \int_A \int_{-h/2}^{h/2} \left(\sigma_x^0 \frac{\partial u_3}{\partial x} \frac{\partial \delta u_3}{\partial x} + 2\sigma_{xy}^0 \frac{\partial u_3}{\partial x} \frac{\partial \delta u_3}{\partial y} + \sigma_y^0 \frac{\partial u_3}{\partial y} \frac{\partial \delta u_3}{\partial y} \right) dz dA \tag{20}$$

where σ_x^0, σ_y^0, τ_{xy}^0 are in-plane stresses, produced due to applied middle plane loads N_x^0, N_y^0, N_{xy}^0, and: $\left(\sigma_x^0, \sigma_y^0, \tau_{xy}^0\right) = \frac{1}{h}\left(N_x^0, N_y^0, N_{xy}^0\right)$.

The virtual kinetic energy can be written in the form:

$$\delta K = \int_A \int_{-h/2}^{h/2} (\dot{u}_1 \delta \dot{u}_1 + \dot{u}_2 \delta \dot{u}_2 + \dot{u}_3 \delta \dot{u}_3) \rho(z) dA dz \tag{21}$$

where the dot-superscript indicates time derivative, e.g. $\dot{u}_1 = \partial u_1 / \partial t$; $\rho(z)$ is the mass density.

By expressing δU_P, δU_F, δV and δK in terms of displacements, then substituting into Eq. (16) and integrating by parts, and then collecting δu_1^0, δu_2^0, δu_3^0, $\delta\theta_1$, $\delta\theta_2$, $\delta\theta_3$, δu_3^*, we obtain the following equations of motion:

$$\begin{aligned}
\delta u_1^0 &: N_{x,x} + N_{xy,y} = I_0 \ddot{u}_1^0 + J_1 \ddot{\theta}_1 - \frac{1}{2} I_2 \ddot{\theta}_{3,x} - \frac{1}{3} I_3 \left(\kappa \ddot{u}_{3,x}^0 + \ddot{u}_{3,x}^* \right); \\
\delta u_2^0 &: N_{xy,x} + N_{y,y} = I_0 \ddot{u}_2^0 + J_1 \ddot{\theta}_2 - \frac{1}{2} I_2 \ddot{\theta}_{3,y} - \frac{1}{3} I_3 \left(\kappa \ddot{u}_{3,y}^0 + \ddot{u}_{3,y}^* \right); \\
\delta u_3^0 &: \frac{\kappa}{3} \left(M_{x,xx}^* + 2M_{xy,xy}^* + M_{y,yy}^* \right) + R_{x,x} + R_{y,y} + f_z^- + \tilde{N}_0 = I_0 \ddot{u}_3^0 + I_1 \ddot{\theta}_3 + I_2 \ddot{u}_3^* \\
&\quad + \frac{I_3 \kappa}{3} \left(\ddot{u}_{1,x}^0 + \ddot{u}_{2,y}^0 \right) + \frac{J_4 \kappa}{3} \left(\ddot{\theta}_{1,x} + \ddot{\theta}_{2,y} \right) - \frac{I_5 \kappa}{6} \nabla^2 \ddot{\theta}_z - \frac{I_6 \kappa^2}{9} \nabla^2 \ddot{w}_0 - \frac{I_6 \kappa}{9} \nabla^2 \ddot{w}_0^*; \\
\delta\theta_1 &: R_x - P_{x,x} - P_{xy,y} = -J_1 \ddot{u}_1^0 - K_2 \ddot{\theta}_1 + \frac{J_3}{2} \ddot{\theta}_{3,x} + \frac{J_4 \kappa}{3} \ddot{u}_{3,x}^0 + \frac{J_4}{3} \ddot{u}_{3,x}^*; \\
\delta\theta_2 &: R_y - P_{xy,x} - P_{y,y} = -J_1 \ddot{u}_2^0 - K_2 \ddot{\theta}_2 + \frac{J_3}{2} \ddot{\theta}_{3,y} + \frac{J_4 \kappa}{3} \ddot{u}_{3,y}^0 + \frac{J_4}{3} \ddot{u}_{3,y}^*; \\
\delta\theta_3 &: \frac{1}{2} \left(N_{x,xx}^* + 2N_{xy,xy}^* + N_{y,yy}^* \right) - N_z - \frac{h}{2} f_z^- + \tilde{N}_1 = I_1 \ddot{u}_3^0 + I_2 \ddot{\theta}_3 + I_3 \ddot{u}_3^* \\
&\quad + \frac{1}{2} I_2 \left(\ddot{u}_{1,x}^0 + \ddot{u}_{2,y}^0 \right) + \frac{J_3}{2} \left(\ddot{\theta}_{1,x} + \ddot{\theta}_{2,y} \right) - \frac{I_4}{4} \nabla^2 \ddot{\theta}_3 - \frac{I_5 \kappa}{6} \nabla^2 \ddot{u}_3^0 - \frac{I_5}{6} \nabla^2 \ddot{u}_3^*; \\
\delta u_3^* &: \frac{1}{3} \left(M_{x,xx}^* + 2M_{xy,xy}^* + M_{y,yy}^* \right) - 2M_z + \frac{h^2}{4} f_z^- + \tilde{N}_2 = I_2 \ddot{u}_3^0 + I_3 \ddot{\theta}_3 + I_4 \ddot{u}_3^* \\
&\quad + \frac{I_3}{3} \left(\ddot{u}_{1,x}^0 + \ddot{u}_{2,y}^0 \right) + \frac{J_4}{3} \left(\ddot{\theta}_{1,x} + \ddot{\theta}_{2,y} \right) - \frac{I_5}{6} \nabla^2 \ddot{\theta}_3 - \frac{I_6 \kappa}{9} \nabla^2 \ddot{u}_3^0 - \frac{I_6}{9} \nabla^2 \ddot{u}_3^*
\end{aligned} \tag{22}$$

where

$$P_x = M_x - \frac{\kappa}{3} M_x^*; P_y = M_y - \frac{\kappa}{3} M_y^*; P_{xy} = M_{xy} - \frac{\kappa}{3} M_{xy}^*;$$

$\nabla^2 = \partial^2/\partial x^2 + \partial^2/\partial y^2$ is Laplacian operator;

Mass moments of inertia (I_i, J_m, K_2) are defined as:

$$\begin{aligned}
I_i &= \int_{-h/2}^{h/2} z^i \rho(z) dz; \quad i = 1 \div 6; \\
J_m &= I_m - \frac{\kappa I_{m+2}}{3}; \quad m = 1, 3, 4; \\
K_2 &= I_2 - \frac{2\kappa I_4}{3} + \frac{\kappa^2 I_6}{9}
\end{aligned} \tag{23}$$

and

$$\begin{aligned}\tilde{N}_i &= N_x^i \frac{\partial^2 w_0}{\partial x^2} + N_x^{i+1} \frac{\partial^2 \theta_z}{\partial x^2} + N_x^{i+2} \frac{\partial^2 w_0^*}{\partial x^2} + N_y^i \frac{\partial^2 w_0}{\partial y^2} + N_y^{i+1} \frac{\partial^2 \theta_z}{\partial y^2} + N_y^{i+2} \frac{\partial^2 w_0^*}{\partial y^2} \\ &+2N_{xy}^i \frac{\partial^2 w_0}{\partial x \partial y} + 2N_{xy}^{i+1} \frac{\partial^2 \theta_z}{\partial x \partial y} + 2N_{xy}^{i+2} \frac{\partial^2 w_0^*}{\partial x \partial y}; \quad i = 0, 1, 2\end{aligned} \tag{24}$$

with

$$\left\{ \tilde{N}_x^i \ \tilde{N}_y^i \ \tilde{N}_{xy}^i \right\} = \frac{1}{h} \int_{-h/2}^{h/2} z^i \left\{ N_x^0 \ N_y^0 \ N_{xy}^0 \right\} dz \tag{25}$$

3 Analytical solution

Consider the rectangular FGSP plate with the geometry shown in Fig. 1, in-plane compressive loads in two directions ($N_x^0 = \gamma_1 N_0$, $N_y^0 = \gamma_2 N_0$, $N_{xy}^0 = 0$) are applied. The simply supported boundary conditions of plate edges are demonstrated as follows:

At edge $x = 0$ and $x = a$:

$$v_0 = 0, \ w_0 = 0, \ \theta_y = 0, \ \theta_z = 0, \ w_0^* = 0, \ M_x = 0, \ M_x^* = 0 \tag{26}$$

At edge $y = 0$ and $y = b$:

$$u_0 = 0, \ w_0 = 0, \ \theta_x = 0, \ \theta_z = 0, \ w_0^* = 0, \ M_y = 0, \ M_y^* = 0 \tag{27}$$

The displacement unknowns are assumed as a double trigonometric series, satisfying the above simply supported boundary condition:

$$\begin{aligned}u_1^0(x, y, t) &= \sum_{m=1}^{\infty} \sum_{n=1}^{\infty} U_{mn} e^{i\omega t} \cos(\alpha x) \sin(\beta y); \\ u_2^0(x, y, t) &= \sum_{m=1}^{\infty} \sum_{n=1}^{\infty} V_{mn} e^{i\omega t} \sin(\alpha x) \cos(\beta y); \\ u_3^0(x, y, t) &= \sum_{m=1}^{\infty} \sum_{n=1}^{\infty} W_{mn} e^{i\omega t} \sin(\alpha x) \sin(\beta y); \\ \theta_1(x, y, t) &= \sum_{m=1}^{\infty} \sum_{n=1}^{\infty} \psi_{xmn} e^{i\omega t} \cos(\alpha x) \sin(\beta y); \\ \theta_2(x, y, t) &= \sum_{m=1}^{\infty} \sum_{n=1}^{\infty} \psi_{ymn} e^{i\omega t} \sin(\alpha x) \cos(\beta y); \\ \theta_3(x, y, t) &= \sum_{m=1}^{\infty} \sum_{n=1}^{\infty} \psi_{zmn} e^{i\omega t} \sin(\alpha x) \sin(\beta y); \\ u_3^*(x, y, t) &= \sum_{m=1}^{\infty} \sum_{n=1}^{\infty} W_{mn}^* e^{i\omega t} \sin(\alpha x) \sin(\beta y)\end{aligned} \tag{28}$$

where $i = \sqrt{-1}$; U_{mn}, V_{mn}, W_{mn}, ψ_{xmn}, ψ_{ymn}, ψ_{zmn}, W_{mn}^* are unknown coefficients; ω is the natural frequency; and m, $n = 1, 2, 3, ...$

Substituting Eq. (28) into Eqs. (22), the analytical solutions can be obtained from:

$$\left(\begin{bmatrix} s_{11} & s_{12} & s_{13} & s_{14} & s_{15} & s_{16} & s_{17} \\ s_{12} & s_{22} & s_{23} & s_{24} & s_{25} & s_{26} & s_{27} \\ s_{13} & s_{32} & s_{33}+k_{33} & s_{34} & s_{35} & s_{36} & s_{37}+k_{37} \\ s_{14} & s_{24} & s_{34} & s_{44} & s_{45} & s_{46} & s_{47} \\ s_{15} & s_{25} & s_{35} & s_{45} & s_{55} & s_{56} & s_{57} \\ s_{16} & s_{26} & s_{36} & s_{46} & s_{56} & s_{66}+k_{66} & s_{67} \\ s_{17} & s_{27} & s_{37}+k_{37} & s_{47} & s_{57} & s_{67} & s_{77}+k_{77} \end{bmatrix} - \omega^2[M]_{7\times 7}\right)\begin{Bmatrix} U_{mn} \\ V_{mn} \\ W_{mn} \\ \psi_{xmn} \\ \psi_{ymn} \\ \psi_{zmn} \\ W^*_{mn} \end{Bmatrix} = \begin{Bmatrix} 0 \\ 0 \\ 0 \\ 0 \\ 0 \\ 0 \\ 0 \end{Bmatrix} \tag{29}$$

in which the coefficients of $[S]$, and $[M]$ are given in the Appendix, and:

$$k_{33} = N_0\left(\gamma_1\alpha^2 + \gamma_2\beta^2\right); \quad k_{37} = k_{66} = \frac{h^2}{12}k_{33}; \quad k_{77} = \frac{h^4}{80}k_{33} \tag{30}$$

By dropping all the inertia terms ($\omega = 0$) in Eq. (29), the buckling loads (N_{bl}) corresponding to buckling modes (m,n) of the plates are obtained. The critical buckling load (N_{cr}) is the minimum value among all buckling loads.

The eigenvalue problem is derived from Eq. (29) by removing all in-plane loads ($N_0 = 0$). The solutions of this equation represent the natural frequencies (ω_{mn}) of the plate for any combination of (m,n) mode numbers. The fundamental natural frequency ω_f of the FSGP plate is the smallest one: $\omega_f = \min\{\omega_{mn}\}$.

4 Numerical results

The Matlab program is developed to conduct numerical examples. The simply supported (SS) FGSP plate resting on the Pasternak substrate is investigated. Input data for aluminum foam [52] are: $\nu = 0.3$, $\rho_{\max} = 2707$ kg/m^3, $G_{\max} = 26.923$ GPa, $E_{\max} = 2G_{\max}(1+\nu)$. Firstly, the precision and effectiveness of the current method are confirmed through a comparison of our results with previously established findings. Next, different investigations will be implemented to evaluate the effect of different parameters on the buckling and vibration characteristics of the FGSP plate. Nondimensional parameters are used in the forms [53–55]:

$$\begin{aligned} &\overline{N} = N_{cr}\frac{a^2}{E_{\max}h^3}; \quad \overline{\omega} = \omega_f h\sqrt{\frac{\rho_{\max}}{E_{\max}}}; \\ &K_0 = k_w\frac{a^4}{E_0h^3}; \quad J_0 = k_{sx}\frac{a^2}{E_0h^3\nu} = k_{sy}\frac{b^2}{E_0h^3\nu}; \quad E_0 = 1 \text{ GPa} \end{aligned} \tag{31}$$

4.1 Validation examples

Three examples are conducted to validate critical buckling loads and frequencies. Because of no work in the open literature relating to 3D solutions for FGSP plate (in drained condition), the efficiency of the proposed quasi-3D theory is indicated by comparison with an isotropic plate. Table 1 listed the nondimensional critical buckling loads and fundamental natural frequencies of SS isotropic square plate ($a = b = 1$ m, $h = 0.1$ m, $E = 151$ GPa, $\nu = 0.3$, $\rho = 3000$ kg/cm^3) with various thickness-to-side ratios, under uniaxial compression ($\gamma_1 = -1$, $\gamma_2 = 0$) at edges $x = 0$, a. The nondimensional formulas are [56, 57]:

$$\hat{N} = N_{cr}\frac{a^2}{\pi^2 D_0}; \quad \hat{\omega} = \frac{\omega_f a^2}{\pi^2}\sqrt{\frac{\rho h}{D_0}}; \quad D_0 = \frac{Eh^3}{12\left(1-\nu^2\right)} \tag{32}$$

The comparison between the present results with the 3D solution of Uymaz and Aydogdu [56, 57] using the Ritz method was also made. A very good agreement can be found from Table 1.

Table 2 presents the next validation for the critical buckling load of SS-FGSP square plates ($a = b = 1$ m) with asymmetric porosity distribution and various porosity coefficients (NUPD-AS, $G_1 = 24$ GPa, $\nu = 0.25$,$B = 0.51$ [58]). The results are collated with those of Rad et al. [20] using FSDT and Levy solutions for various thickness-to-side ratios and different porosity coefficients. Good agreements between the obtained results for FGSP plates can be observed, and the discrepancy is acceptable due to using different theories (FSDT and present quasi-3D theory).

Table 1 Validation of nondimensional critical buckling load $\hat{N}$ and nondimensional fundamental natural frequency $\hat{\omega}$ of the isotropic square plate

	Source	*h/a*		
		0.05	0.1	0.2
$\hat{N}$	3D (Ritz) [56]	3.9499	3.8099	3.3299
	Present	3.9471	3.7966	3.2947
	Discrepancy (%)	0.07	0.35	1.06
$\hat{\omega}$	3D (Ritz) [57]	1.9570	1.9339	1.7748
	Present	1.9828	1.9342	1.7760
	Discrepancy (%)	1.32	0.02	0.07

Table 2 Validation of critical buckling load N_{cr} (MN/m) of SS-FGSP square plate (asymmetric porosity distribution)

(γ_1, γ_2)	*h/a*	Source	e_0			
			0	0.3	0.5	0.7
$\gamma_1 = -1$, $\gamma_2 = 0$	0.1	Rad et al. [20]	200.023	167.163	141.292	109.823
		Present	200.443	171.095	146.354	115.004
		Discrepancy (%)	0.21	2.35	3.58	4.72
	0.2	Rad et al. [20]	1391.442	1157.871	978.262	764.934
		Present	1401.846	1187.36	1012.9	799.4139
		Discrepancy (%)	0.75	2.55	3.54	4.51
$\gamma_1 = -1$, $\gamma_2 = -1$	0.1	Rad et al. [20]	100.011	83.582	70.646	54.912
		Present	100.221	85.547	73.177	57.502
		Discrepancy (%)	0.21	2.35	3.58	4.72
	0.2	Rad et al. [20]	695.721	578.936	489.131	382.467
		Present	700.923	593.680	506.450	399.707
		Discrepancy (%)	0.75	2.55	3.54	4.51

Table 3 Nondimensional fundamental natural frequencies ϖ of SS-FGSP square plates with non-uniform asymmetric porosity distribution

B	Sources	*a/h* = 5	*a/h* = 10	*a/h* = 20
0.1	Ebrahim and Habibi [59]	0.21275	0.05783	0.01473
	Present	0.21152	0.05745	0.01471
	Discrepancy (%)	0.58	0.66	0.13
0.3	Ebrahim and Habibi [59]	0.21563	0.05876	0.01495
	Present	0.21445	0.05833	0.01494
	Discrepancy (%)	0.55	0.73	0.04
0.5	Ebrahim and Habibi [59]	0.21857	0.05954	0.01526
	Present	0.21728	0.05919	0.01517
	Discrepancy (%)	0.59	0.59	0.58
0.7	Ebrahim and Habibi [59]	0.22162	0.06055	0.01549
	Present	0.22002	0.06002	0.01539
	Discrepancy (%)	0.72	0.87	0.64

The last validation is conducted for nondimensional fundamental natural frequencies $\overline{\omega}$ of SS-FGSP square NUPD-AS plates ($E_1 = 69$ GPa, $\rho_1 = 2260$ kg/m^3, $\nu = 0.25$ [7], $e_0 = 0$, $K_0 = J_0 = 0$). Table 3 presented the comparison between the present results and those of Ebrahimi and Habibi [59], which used the FEM and Reddy's TSDT [60]. Remarkable consistency is evident for all *a/h* ratios (the maximum discrepancy is only 0.87%).

Through validated examples, it can be concluded that the proposed quasi-3D HSDT can be trustfully employed to explore the buckling response and free vibrational characteristic of thick FGSP plates.

4.2 Buckling analysis

Consider rectangular SS-FGSP (aluminum foam), subjected to in-plane uni-axial ($\gamma_1 = -1$, $\gamma_2 = 0$) and bi-axial ($\gamma_1 = \gamma_2 = -1$) uniform compressive loads: $N_x^0 = \gamma_1 N_{cr}$, $N_y^0 = \gamma_2 N_{cr}$.

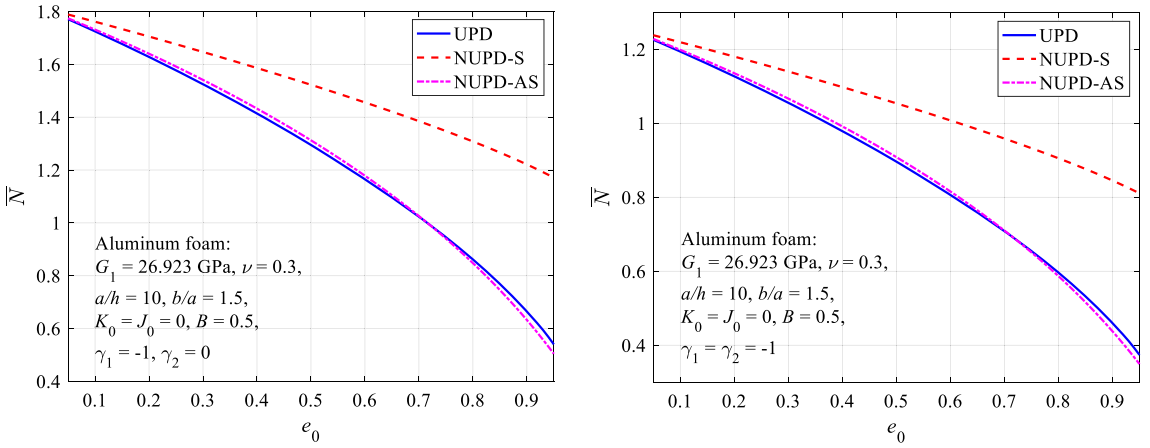

Fig. 2 Effect of porosity variation types and porosity coefficient on the non-dimensional critical buckling load of SS-FGSP plates

Table 4 Nondimensional critical buckling load of SS-FGSP plates with different Skempton coefficient B and porosity coefficient e_0

B	e_0			
	0.1	0.3	0.5	0.8
0.1	1.1856	1.0330	0.8617	0.5391
0.3	1.1921	1.0500	0.8854	0.5632
0.5	1.1986	1.0668	0.9086	0.5869
0.8	1.2084	1.0917	0.9431	0.6230

Figure 2 shows the effect of porosity variation types and porosity coefficient of FGP materials on the non-dimensional critical buckling load of FGSP plates. It can be observed that an increase in the porosity coefficient e_0 makes the plate softer, leading to a decrease in the nondimensional critical buckling load for all porosity variation types. It can be also seen that the FGSP plate with nonuniform symmetric distribution pattern (NUPD-S) is the stiffest and thus has the highest critical buckling load, while the remaining two distribution patterns (UPD and NUPD-AS) have almost the same stiffness (withstand lower critical buckling loads and have similar values).

The influence of Skempton coefficient B on the non-dimensional critical buckling load of FGSP plates without elastic foundation (NUPD-S, $\gamma_1 = \gamma_2 = -1$, $a/h = 10$, $b/a = 1.5$) is depicted in Table 4 and Fig. 3. The findings indicate that a higher Skempton coefficient B leads to a slight increase in the nondimensional critical buckling load. The increased pore pressure leads to a higher equivalent stiffness of the plate, explaining this observation. Furthermore, the effect of Skempton coefficient B is more pronounced as the porosity coefficient e_0 is larger. For example, with $e_0 = 0.95$, when $B = 0.05$: $\overline{N} = 0.3120$; when $B = 0.95$: $\overline{N} = 0.3922$ (increase 25.72%).

Figure 4 exhibits the relationship between the non-dimensional critical buckling load of FGSP plates (NUPD-S, $B = 0.5$, $e_0 = 0.5$, $\gamma_1 = \gamma_2 = -1$, $h = 0.1$ m) versus a/h as well as b/a ratios. This figure also shows that non-dimensional critical buckling load rises as the a/h ratio increases but declines as the b/a ratio increases. This figure also reveals that non-dimensional critical buckling load increases with increasing a/h ratio, but decreases with increasing b/a ratio.

The relationship between the non-dimensional critical buckling load of rectangular ($a/h = 10$, $b/a = 1.5$) FGSP (NUPD-S,$B = 0.5$, $e_0 = 0.5$, $\gamma_1 = \gamma_2 = -1$) plates and elastic foundation parameters is shown in Fig. 5. It is clear that the attendance of an elastic foundation enhances the stability of FGSP plates, as evidenced by the increased critical buckling loads. Results further show that a higher value for the elastic foundation coefficients leads to an increase in the non-dimensional critical buckling load. Furthermore, the Pasternak foundation coefficient J_0 has a more significant impact compared to the Winkler foundation coefficient K_0.

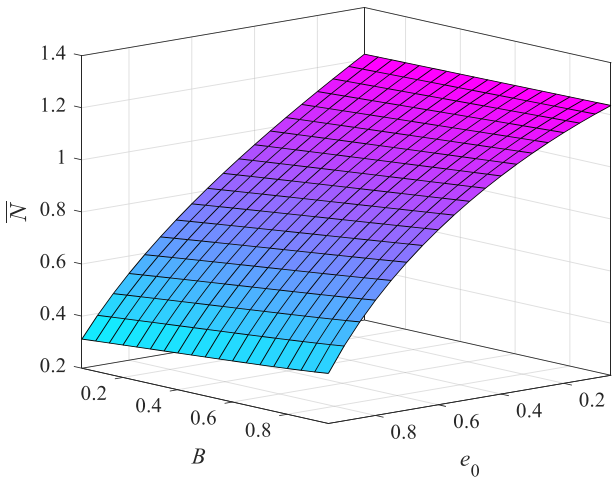

Fig. 3 The relationship between the non-dimensional critical buckling load $\overline{N}$ of FGSP plates (NUPD-S) and parameters$B$ and e_0

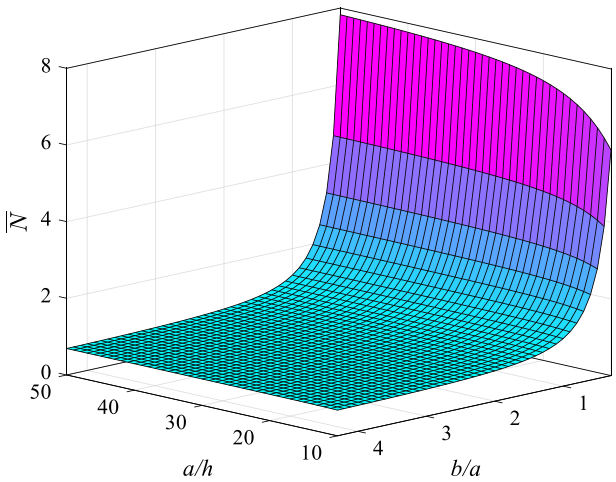

Fig. 4 The relationship between the non-dimensional critical buckling load $\overline{N}$ of FGSP plates (NUPD-S) and a/h and b/a ratios

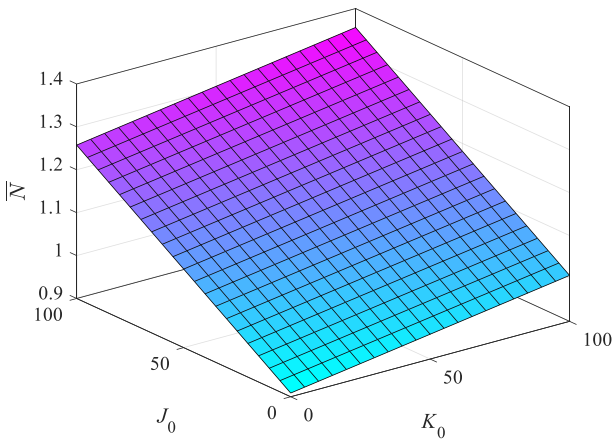

Fig. 5 The relationship between the non-dimensional critical buckling load $\overline{N}$ of FGSP plates and elastic foundation parameters

Table 5 The nondimensional fundamental natural frequencies SS-FGSP (NUPD-S, $a/h = 10$, $b/a = 1.5$) plate with different Skempton coefficient B and porosity coefficient e_0

B	e_0			
	0.1	0.3	0.5	0.8
0.1	0.0416	0.0403	0.0386	0.0342
0.3	0.0417	0.0406	0.0392	0.0350
0.5	0.0418	0.0410	0.0397	0.0357
0.8	0.0420	0.0414	0.0404	0.0368

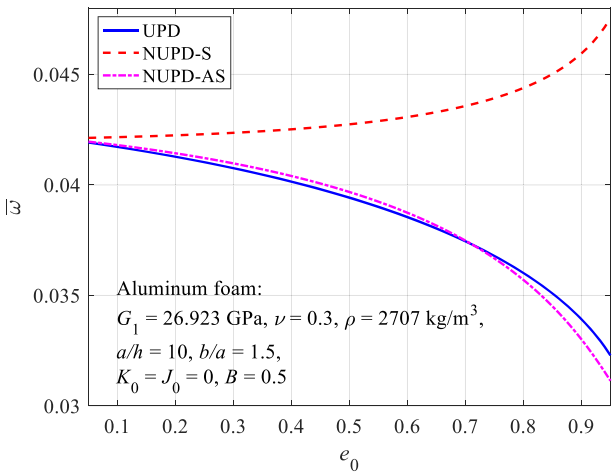

Fig. 6 Change of non-dimensional fundamental natural frequencies $\overline{\omega}$ of FGSP plates (NUPD-S) versus e_0 coefficient

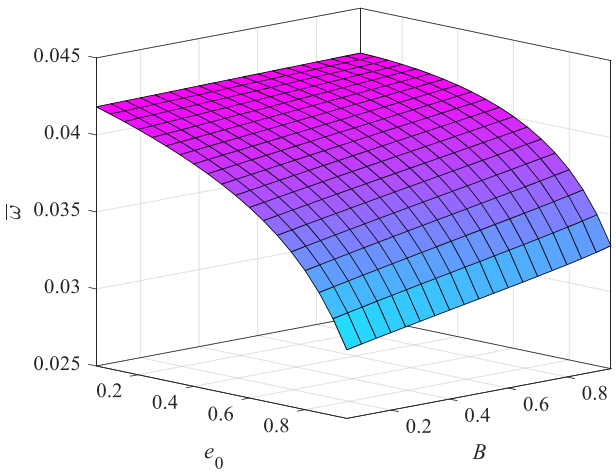

Fig. 7 Change of non-dimensional fundamental natural frequencies $\overline{\omega}$ of FGSP plates (NUPD-S) versus$B$ and e_0

4.3 Free vibration analysis

Table 5 and Figs. 6, 7, 8, and 9 show the impact of porosity distribution types and porosity coefficient, Skempton pore pressure coefficient B of FGSP materials, and geometrical and elastic foundation coefficients on nondimensional fundamental natural frequencies of SS-FGSP plates.

From Fig. 6 can be seen that for UPD and NUPD-AS when e_0 increases, the free space of the FGSP plate rises, resulting in a decrease in the stiffness of the plate, which, in turn, leads to a reduction in the nondimensional fundamental natural frequencies. However, for NUPD-S, the variation tendency of nondimensional fundamental natural frequency is the opposite, when e_0 increases, the frequency increases. This phenomenon can be explained by the correlation between the mass effect and the bending stiffness of the plate. Additionally,

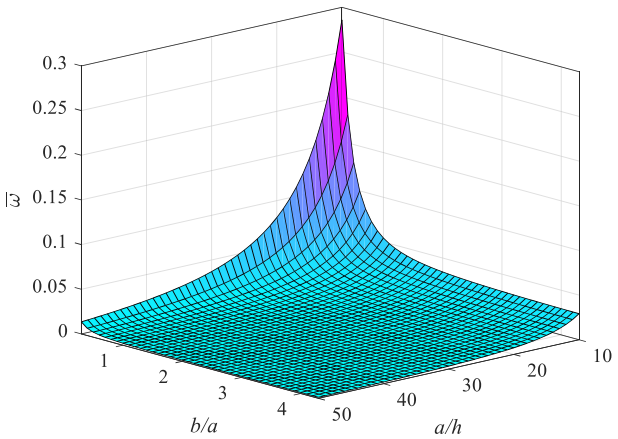

Fig. 8 Variation of nondimensional fundamental natural frequencies $\overline{\omega}$ of FGSP plates versus *a/h* and *b/a* ratios

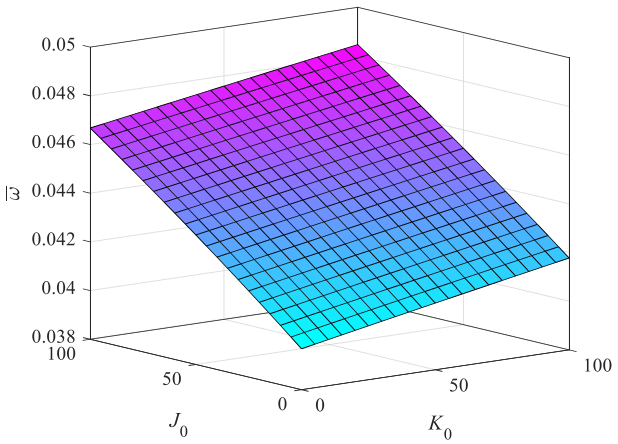

Fig. 9 Effect of elastic foundation parameters on nondimensional fundamental natural frequencies $\overline{\omega}$ of FGSP plates

the influence of porosity distribution becomes more pronounced with increasing porosity coefficient. This is evident from the larger gaps between curves corresponding to different porosity patterns.

Table 5 and Fig. 7 describe the relationship between the Skempton pore pressure coefficient and the nondimensional fundamental natural frequencies. It can be seen that as the Skempton coefficient B rises, it increases the natural frequency. This is due to the fact that by increasing the Skempton coefficient, the compressibility of fluid within the pores decreases and the natural frequencies increase. The influence of coefficient B is more significant when the porosity coefficient e_0 is larger. For example, with $e_0 = 0.95$: $\overline{\omega} = 0.0295$ when $B = 0.05$; and $\overline{\omega} = 0.0330$ when $B = 0.95$ (an increase of 11.97%).

The impact of geometrical parameters on the natural frequencies $\overline{\omega}$ of FGSP plates without elastic foundation (NUPD-S, $B = 0.5$, $e_0 = 0.5$) can be indicated in Fig. 8. As the thickness-to-side ratio *a/h* increases (plate becomes thinner), the nondimensional fundamental natural frequency decreases motonically. The nondimensional fundamental natural frequency exhibits a decrease with increasing aspect ratio. This decrease is most pronounced for small values of the *b/a* ratio. As the b/a ratio increases, the rate of decrease becomes more gradual. For example, at an aspect ratio *a/h* at 10: when $b/a = 1$, the nondimensional fundamental natural frequency $\overline{\omega}$ is 0.0544. Doubling the *b/a* ratio to 2 reduces $\overline{\omega}$ to 0.0345 (a 1.58-fold decrease), at $b/a = 4$, $\overline{\omega}$ further decreases to 0.00294 (a 1.17-fold decrease compared to $b/a = 2$).

Figure 9 illustrates the impact of foundation coefficients on natural frequencies $\overline{\omega}$ of FGSP (NUPD-S, $B = 0.5$, $e_0 = 0.5$) rectangular plates ($a/h = 10$; $b/a = 1.5$) have the same trend as the above-mentioned in buckling analysis. The fundamental natural frequency increases as foundation parameters increase, and the Pasternak foundation parameter affects natural frequency more significantly than Winkler foundation parameters.

5 Conclusion

In this paper, the new quasi-3D HSDT is employed to explore the buckling behavior and free vibrational characteristic of FGSP plates for the first time. This quasi-3D theory satisfies zeros stress-free conditions on the top and bottom surfaces of the plate and simultaneously considers both transverse normal strain and transverse shear strains. The model shows high similarity to the 3D solution, making it suitable for thick plate analysis. Three porosity variation types are considered, in which the non-uniform distributions are described by simple cosine law. Based on Navier's technique, the critical buckling loads and natural frequencies of SS-FGSP plates are determined. The accuracy of the proposed model is confirmed by comparison with the solution given by 3D elasticity theory for isotropic plate and within the framework of the HSDT solution for drained and undrained functionally grade porous plate. A comprehensive investigation is performed to highlight the impact of porosity, saturation, geometrical, and elastic foundation parameters on FGSP plate response. The major findings are listed below:

- The increased porosity coefficient reduces the stiffness of FGSP plates, resulting in a decrease in the uniaxial, and biaxial critical buckling loads for all types of porosity distribution. Due to the relative correlation between mass effect and plate stiffness, the fundamental natural frequency decreases as the porosity coefficient increases for UPD and NUPD-AS plates, and vice versa for the NUPD-S plate.
- The porosity distribution patterns affect significantly the buckling and free vibration behavior of FGSP plates. For a certain value of porosity coefficient, the NUPD-S plate provided the highest critical buckling loads and fundamental natural frequencies, UPD and NUPD-AS plates provided smaller ones and their values are close. Moreover, the influence of porosity distribution patterns becomes increasingly noticeable as the porosity coefficient rises.
- Increasing the Skempton pore pressure coefficient B caused a decrease in the compressibility of fluid within the pores, leading to an increase in critical buckling load and fundamental natural frequency. This increment is greater as the Skempton coefficient increases.
- When the *a/h* ratio is increased, the nondimensional critical buckling loads rise but nondimensional fundamental natural frequencies decrease. Conversely, when the *b/a* ratio is increased, the nondimensional critical buckling load and fundamental natural frequency decrease.
- The elastic foundation plays a substantial role in influencing critical buckling loads and fundamental natural frequencies. Specifically, the impact of the Pasternak foundation coefficient J_0 is more prominent than that of the Winkler foundation coefficient K_0.

Acknowledgements This research is funded by Vietnam's National Foundation for Science and Technology Development (NAFOSTED) under grant number: 107.02-2021.16.

Author contributions Vu Thi Thu Trang: Methodology, Supervision, Writing – original draft. Nguyen Van Long: Methodology, Project administration, Software, Writing – original draft, Writing – review & editing. Tran Minh Tu: Formal analysis, Software, Supervision, Writing – review & editing. Le Thanh Hai: Data curation, Investigation, Validation, Writing – review & editing.

Declarations

Conflict of interest The authors declare no competing interests.

Appendix: The global linear stiffness matrix [S], and global mass matrix [M] Coefficients of matrix [S]:

$$s_{11} = A_1\alpha^2 + A_3\beta^2; s_{12} = (A_2 + A_3)\alpha\beta; s_{13} = -\frac{D_1}{3}\kappa\alpha^3 - \left(\frac{D_2}{3} + \frac{2D_3}{3}\right)\kappa\alpha\beta^2;$$

$$s_{14} = \left(B_1 - \frac{D_1\kappa}{3}\right)\alpha^2 + \left(B_3 - \frac{D_3\kappa}{3}\right)\beta^2; s_{15} = \left(B_2 + B_3 - \frac{D_2\kappa}{3} - \frac{D_3\kappa}{3}\right)\alpha\beta;$$

$$s_{16} = s_{61} = -\frac{C_1}{2}\alpha^3 - A_2\alpha - \left(\frac{C_2}{2} + C_3\right)\alpha\beta^2; s_{17} = -\frac{D_1}{3}\alpha^3 - 2B_2\alpha - \left(\frac{D_2}{3} + \frac{2D_3}{3}\right)\alpha\beta^2;$$

$$s_{22} = A_3\alpha^2 + A_1\beta^2; s_{23} = -\left(\frac{D_2}{3} + \frac{2D_3}{3}\right)\kappa\alpha^2\beta - \frac{D_1}{3}\kappa\beta^3;$$

$$s_{24} = \left(B_2 + B_3 - \frac{D_2\kappa}{3} - \frac{D_3\kappa}{3}\right)\alpha\beta; s_{25} = \left(B_3 - \frac{D_3\kappa}{3}\right)\alpha^2 + \left(B_1 - \frac{D_1\kappa}{3}\right)\beta^2;$$

$$s_{26} = -\left(\frac{C_2}{2} + C_3\right)\alpha^2\beta - A_2\beta - \frac{C_1}{2}\beta^3; s_{27} = -\left(\frac{D_2}{3} + \frac{2D_3}{3}\right)\alpha^2\beta - 2B_2\beta - \frac{D_1}{3}\beta^3;$$

$$s_{33} = \frac{G_1\kappa^2}{9}\alpha^4 + A^s\alpha^2 + \frac{2(G_2 + 2G_3)\kappa^2}{9}\alpha^2\beta^2 + A^s\beta^2 + \frac{G_1\kappa^2}{9}\beta^4 + \xi;$$

$$s_{34} = \left(\frac{G_1\kappa^2}{9} - \frac{E_1\kappa}{3}\right)\alpha^3 + A^s\alpha - \left(\frac{E_2\kappa}{3} + \frac{2E_3\kappa}{3} - \frac{G_2\kappa^2}{9} - \frac{2G_3\kappa^2}{9}\right)\alpha\beta^2;$$

$$s_{35} = s_{53} = -\left(\frac{E_2\kappa}{3} + \frac{2E_3\kappa}{3} - \frac{G_2\kappa^2}{9} - \frac{2G_3\kappa^2}{9}\right)\alpha^2\beta + A^s\beta + \left(\frac{G_1\kappa^2}{9} - \frac{E_1\kappa}{3}\right)\beta^3;$$

$$s_{36} = \frac{F_1\kappa}{6}\alpha^4 + \frac{D_2\kappa}{3}\alpha^2 + \left(\frac{F_2}{3} - \frac{2F_3}{3}\right)\kappa\alpha^2\beta^2 + \frac{D_2\kappa}{3}\beta^2 + \frac{F_1\kappa}{6}\beta^4 - \frac{h}{2}\xi;$$

$$s_{37} = \frac{G_1\kappa}{9}\alpha^4 + \frac{2E_2\kappa}{3}\alpha^2 + \left(\frac{2G_2}{9} + \frac{4G_3}{9}\right)\kappa\alpha^2\beta^2 + \frac{2E_2\kappa}{3}\beta^2 + \frac{G_1\kappa}{9}\beta^4 + \frac{h^2}{4}\xi;$$

$$s_{44} = \left(\frac{G_1\kappa^2}{9} - \frac{2E_1\kappa}{3} + C_1\right)\alpha^2 + \left(\frac{G_3\kappa^2}{9} - \frac{2E_3\kappa}{3} + C_3\right)\beta^2 + A^s;$$

$$s_{45} = s_{54} = \left(C_2 + C_3 + \frac{G_2\kappa^2}{9} + \frac{G_3\kappa^2}{9} - \frac{2E_2\kappa}{3} - \frac{2E_3\kappa}{3}\right)\alpha\beta;$$

$$s_{46} = -\left(\frac{D_1}{2} - \frac{F_1\kappa}{6}\right)\alpha^3 + \left(\frac{D_2\kappa}{3} - B_2\right)\alpha - \left(\frac{D_2}{2} + D_3 - \frac{F_2\kappa}{6} - \frac{F_3\kappa}{3}\right)\alpha\beta^2;$$

$$s_{47} = -\left(\frac{E_1}{3} - \frac{G_1\kappa}{9}\right)\alpha^3 + \left(\frac{2E_2\kappa}{3} - 2C_2\right)\alpha - \left(\frac{E_2}{3} + \frac{2E_3}{3} - \frac{G_2\kappa}{9} - \frac{2G_3\kappa}{9}\right)\alpha\beta^2;$$

$$s_{55} = \left(\frac{G_3\kappa^2}{9} - \frac{2E_3\kappa}{3} + C_3\right)\alpha^2 + \left(\frac{G_1c_0^2}{9} - \frac{2E_1\kappa}{3} + C_1\right)\beta^2 + A^s;$$

$$s_{56} = -\left(\frac{D_2}{2} + D_3 - \frac{F_2\kappa}{6} - \frac{F_3\kappa}{3}\right)\alpha^2\beta + \left(\frac{D_2\kappa}{3} - B_2\right)\beta - \left(\frac{D_1}{2} - \frac{F_1\kappa}{6}\right)\beta^3;$$

$$s_{57} = -\left(\frac{E_2}{3} + \frac{2E_3}{3} - \frac{G_2\kappa}{9} - \frac{2G_3\kappa}{9}\right)\alpha^2\beta + \left(\frac{2E_2\kappa}{3} - 2C_2\right)\beta - \left(\frac{E_1}{3} - \frac{G_1\kappa}{9}\right)\beta^3;$$

$$s_{66} = \frac{E_1}{4}\alpha^4 + C_2\alpha^2 + \left(\frac{E_2}{2} + E_3\right)\alpha^2\beta^2 + C_2\beta^2 + \frac{E_1}{4}\beta^4 + A_1 + \frac{h^2}{4}\xi;$$

$$s_{67} = \frac{F_1}{6}\alpha^4 + 2D_2\alpha^2 + \left(\frac{F_2}{3} + \frac{2F_3}{3}\right)\alpha^2\beta^2 + 2D_2\beta^2 + \frac{F_1}{6}\beta^4 + 2B_1 - \frac{h^3}{8}\xi;$$

$$s_{77} = \frac{G_1}{9}\alpha^4 + \frac{4E_2}{3}\alpha^2 + \left(\frac{2G_2}{9} + \frac{4G_3}{9}\right)\alpha^2\beta^2 + \frac{4E_2}{3}\beta^2 + \frac{G_1}{9}\beta^4 + 4C_1 + \frac{h^4}{16}\xi;$$

with $\xi = k_w + k_{sx}\alpha^2 + k_{sy}\beta^2$.

Coefficients of matrix [M]:

$$[M] = \begin{bmatrix} m_{11} & 0 & m_{13} & m_{14} & 0 & m_{16} & m_{17} \\ 0 & m_{22} & m_{23} & 0 & m_{25} & m_{26} & m_{27} \\ m_{13} & m_{23} & m_{33} & m_{34} & m_{35} & m_{36} & m_{37} \\ m_{14} & 0 & m_{34} & m_{44} & 0 & m_{46} & m_{47} \\ 0 & m_{25} & m_{35} & 0 & m_{55} & m_{56} & m_{57} \\ m_{16} & m_{26} & m_{36} & m_{46} & m_{56} & m_{66} & m_{67} \\ m_{17} & m_{27} & m_{37} & m_{47} & m_{57} & m_{67} & m_{77} \end{bmatrix};$$

$$m_{11} = m_{22} = I_0; m_{13} = -\frac{\alpha\kappa}{3} I_3; m_{14} = J_1; m_{16} = -\frac{\alpha}{2} I_2; m_{17} = -\frac{\alpha}{3} I_3;$$

$$m_{23} = -\frac{\beta\kappa}{3} I_3; m_{25} = J_1; m_{26} = -\frac{\beta}{2} I_2; m_{27} = -\frac{\beta}{3} I_3;$$

$$m_{33} = I_0 + \frac{\left(\alpha^2 + \beta^2\right)\kappa^2}{9} I_6; m_{34} = -\frac{\alpha\kappa}{3} J_4; m_{35} = -\frac{\beta\kappa}{3} J_4;$$

$$m_{36} = I_1 + \frac{\left(\alpha^2 + \beta^2\right)\kappa}{6} I_5; m_{37} = I_2 + \frac{\left(\alpha^2 + \beta^2\right)\kappa}{9} I_6; m_{44} = m_{55} = K_2;$$

$$m_{46} = -\frac{\alpha}{2} J_3; m_{47} = -\frac{\alpha}{3} J_4; m_{56} = -\frac{\beta}{2} J_3; m_{57} = -\frac{\beta}{3} J_4;$$

$$m_{66} = I_2 + \frac{\left(\alpha^2 + \beta^2\right)}{4} I_4; m_{67} = I_3 + \frac{\left(\alpha^2 + \beta^2\right)}{6} I_5; m_{77} = I_4 + \frac{\left(\alpha^2 + \beta^2\right)}{9} I_6.$$

References

1. Biot, M.A.: Theory of elasticity and consolidation for a porous anisotropic solid. J. Appl. Phys. **26**(2), 182–185 (1955)
2. Arefi, M., Meskini, M.: Application of hyperbolic shear deformation theory to free vibration analysis of functionally graded porous plate with piezoelectric face-sheets. Struct. Eng. Mech. **71**(5), 459–467 (2019)
3. Ghorbanpour Arani, A., Khani, M., Khoddami Maraghi, Z.: Dynamic analysis of a rectangular porous plate resting on an elastic foundation using high-order shear deformation theory. J. Vib. Control. Vib. Control **24**(16), 3698–3713 (2018)
4. Tu, T.M., Hoa, L.K., Hung, D.X., Hai, L.T.: Nonlinear buckling and post-buckling analysis of imperfect porous plates under mechanical loads. J. Sandwich Struct. Mater. **22**(6), 1910–1930 (2020)
5. Zghal, S., Dammak, F.: Buckling responses of porous structural components with gradient power-based and sigmoid material variations under different types of compression loads. Compos. Struct. **273**, 114313 (2021)
6. Theodorakopoulos, D., Beskos, D.: Flexural vibrations of poroelastic plates. Acta Mech. **103**(1), 191–203 (1994)
7. Leclaire, P., Horoshenkov, K., Cummings, A.: Transverse vibrations of a thin rectangular porous plate saturated by a fluid. J. Sound Vib. **247**(1), 1–18 (2001)
8. Jabbari, M., Mojahedin, A., Khorshidvand, A.R., Eslami, M.R.: Buckling analysis of a functionally graded thin circular plate made of saturated porous materials. J. Eng. Mech. **140**(2), 287–295 (2014)
9. Jabbari, M., Hashemitaheri, M., Mojahedin, A., Eslami, M.R.: Thermal buckling analysis of functionally graded thin circular plate made of saturated porous materials. J. Therm. Stresses **37**(2), 202–220 (2014)
10. Jabbari, M., Mojahedin, A., Joubaneh, E.F.: Thermal buckling analysis of circular plates made of piezoelectric and saturated porous functionally graded material layers. J. Eng. Mech. **141**(4), 04014148 (2015)
11. Jabbari, M., Rezaei, M., Mojahedin, A.: Mechanical buckling of FG saturated porous rectangular plate with piezoelectric actuators. Iran. J. Mech. Eng. Trans. ISME **17**(2), 46–66 (2016)
12. Rezaei, A., Saidi, A.: An analytical study on the free vibration of moderately thick fluid-infiltrated porous annular sector plates. J. Vib. Control **24**(18), 4130–4144 (2018)
13. Rezaei, A., Saidi, A.: Buckling response of moderately thick fluid-infiltrated porous annular sector plates. Acta Mech. **228**(11), 3929–3945 (2017)
14. Rezaei, A., Saidi, A.: On the effect of coupled solid-fluid deformation on natural frequencies of fluid saturated porous plates. Eur. J. Mech. A/Solids **63**, 99–109 (2017)
15. Chen, D., Yang, J., Kitipornchai, S.: Buckling and bending analyses of a novel functionally graded porous plate using Chebyshev–Ritz method. Arch. Civ. Mech. Eng. **19**(1), 157–170 (2019)
16. Zhao, J., Wang, Q., Deng, X., Choe, K., Zhong, R., Shuai, C.: Free vibrations of functionally graded porous rectangular plate with uniform elastic boundary conditions. Compos. B Eng. **168**, 106–120 (2019)
17. Bemani Khouzestani, L., Khorshidvand, A.R.: Axisymmetric free vibration and stress analyses of saturated porous annular plates using generalized differential quadrature method. J. Vib. Control. Vib. Control **25**(21–22), 2799–2818 (2019)
18. Sharifan, M.H., Jabbari, M.: Mechanical buckling analysis of saturated porous functionally graded elliptical plates subjected to in-plane force resting on two parameters elastic foundation based on HSDT. J. Pressure Vessel Technol. **142**(4), 041302 (2020)
19. Mojahedin, A., Jabbari, M., Khorshidvand, A.R., Eslami, M.R.: Buckling analysis of functionally graded circular plates made of saturated porous materials based on higher order shear deformation theory. Thin Wall. Struct. **99**, 83–90 (2016)

20. Rad, E.S., Saidi, A.R., Rezaei, A.S., Askari, M.: Shear deformation theories for elastic buckling of fluid-infiltrated porous plates: an analytical approach. Compos. Struct. **254**, 112829 (2020)
21. Rezaei, A., Saidi, A.: Exact solution for free vibration of thick rectangular plates made of porous materials. Compos. Struct. **134**, 1051–1060 (2015)
22. Kiarasi, F., Babaei, M., Asemi, K., Dimitri, R., Tornabene, F.: Three-dimensional buckling analysis of functionally graded saturated porous rectangular plates under combined loading conditions. Appl. Sci. **11**(21), 10434 (2021)
23. Babaei, M., Asemi, K., Kiarasi, F.: Static response and free-vibration analysis of a functionally graded annular elliptical sector plate made of saturated porous material based on 3D finite element method. Mech. Based Des. Struct. Mach.. Based Des. Struct. Mach. **51**, 1–25 (2020)
24. Babaei, M., Hajmohammad, M.H., Asemi, K.: Natural frequency and dynamic analyses of functionally graded saturated porous annular sector plate and cylindrical panel based on 3D elasticity. Aerosp. Sci. Technol. **96**, 105524 (2020)
25. Carrera, E., Brischetto, S., Cinefra, M., Soave, M.: Effects of thickness stretching in functionally graded plates and shells. Compos. B Eng. **42**(2), 123–133 (2011)
26. Bouafia, K., Selim, M.M., Bourada, F., Bousahla, A.A., Bourada, M., Tounsi, A., Bedia, E.A.A., Tounsi, A.: Bending and free vibration characteristics of various compositions of FG plates on elastic foundation via quasi 3D HSDT model. Steel Compos. Struct. Int. J. **41**(4), 487–503 (2021)
27. Lafi, D.E., Bouhadra, A., Mamen, B., Menasria, A., Bourada, M., Bousahla, A.A., Bourada, F., Tounsi, A., Tounsi, A., Yaylaci, M.: Combined influence of variable distribution models and boundary conditions on the thermodynamic behavior of FG sandwich plates lying on various elastic foundations. Struct. Eng. Mech. **89**(2), 103 (2024)
28. Zaitoun, M.W., Chikh, A., Tounsi, A., Al-Osta, M.A., Sharif, A., Al-Dulaijan, S.U., Al-Zahrani, M.M.: Influence of the visco-Pasternak foundation parameters on the buckling behavior of a sandwich functional graded ceramic–metal plate in a hygrothermal environment. Thin Wall. Struct. **170**, 108549 (2022)
29. Tahir, S.I., Tounsi, A., Chikh, A., Al-Osta, M.A., Al-Dulaijan, S.U., Al-Zahrani, M.M.: The effect of three-variable viscoelastic foundation on the wave propagation in functionally graded sandwich plates via a simple quasi-3D HSDT. Steel Compos. Struct. **42**(4), 501 (2022)
30. Zaitoun, M.W., Chikh, A., Tounsi, A., Sharif, A., Al-Osta, M.A., Al-Dulaijan, S.U., Al-Zahrani, M.M.: An efficient computational model for vibration behavior of a functionally graded sandwich plate in a hygrothermal environment with viscoelastic foundation effects. Eng. Comput. **39**(2), 1127–1141 (2023)
31. Bennedjadi, M., Aldosari, S.M., Chikh, A., Kaci, A., Bousahla, A.A., Bourada, F., Tounsi, A., Benrahou, K.H., Tounsi, A.: Visco-elastic foundation effect on buckling response of exponentially graded sandwich plates under various boundary conditions. Geomech. Eng. **32**(2), 159 (2023)
32. Bounouara, F., Aldosari, S.M., Chikh, A., Kaci, A., Bousahla, A.A., Bourada, F., Tounsi, A., Benrahou, K.H., Albalawi, H., Tounsi, A.: The effect of visco-Pasternak foundation on the free vibration behavior of exponentially graded sandwich plates with various boundary conditions. Steel Compos. Struct. Int. J. **46**(3), 367–383 (2023)
33. Mudhaffar, I.M., Chikh, A., Tounsi, A., Al-Osta, M.A., Al-Zahrani, M.M., Al-Dulaijan, S.U.: Impact of viscoelastic foundation on bending behavior of FG plate subjected to hygro-thermo-mechanical loads. Struct. Eng. Mech. Int. J. **86**(2), 167–180 (2023)
34. Tounsi, A., Mostefa, A.H., Bousahla, A.A., Tounsi, A., Ghazwani, M.H., Bourada, F., Bouhadra, A.: Thermodynamical bending analysis of P-FG sandwich plates resting on nonlinear visco-Pasternak's elastic foundations. Steel Compos. Struct. **49**(3), 307–323 (2023)
35. Tounsi, A., Mostefa, A.H., Attia, A., Bousahla, A.A., Bourada, F., Tounsi, A., Al-Osta, M.A.: Free vibration investigation of functionally graded plates with temperaturedependent properties resting on a viscoelastic foundation. Struct. Eng. Mech. Int. J. **86**(1), 1–16 (2023)
36. Tounsi, A., Bousahla, A.A., Tahir, S.I., Mostefa, A.H., Bourada, F., Al-Osta, M.A., Tounsi, A.: Influences of different boundary conditions and hygro-thermal environment on the free vibration responses of FGM sandwich plates resting on viscoelastic foundation. Int. J. Struct. Stab. Dyn. 2450117 (2023)
37. Gawah, Q., Bourada, F., Al-Osta, M. A., Tahir, S. I., Tounsi, A., Yaylacı, M.: An improved first-order shear deformation theory for wave propagation analysis in FG-CNTRC beams resting on a viscoelastic substrate (2024)
38. Neves, A., Ferreira, A.J.M., Carrera, E., Cinefra, M., Roque, C.M.C., Jorge, R.M.N., Soares, C.M.: Static, free vibration and buckling analysis of isotropic and sandwich functionally graded plates using a quasi-3D higher-order shear deformation theory and a meshless technique. Compos. B Eng. **44**(1), 657–674 (2013)
39. Mashat, D.S., Zenkour, A.M., Radwan, A.F.: A quasi-3D higher-order plate theory for bending of FG plates resting on elastic foundations under hygro-thermo-mechanical loads with porosity. Eur. J. Mech. A. Solids **82**, 103985 (2020)
40. Tru, V.N., Long, N.V., Tu, T.M., Trang, V.T.T.: Static analysis of functionally graded saturated porous plate rested on Pasternak elastic foundation by using a new quasi-3D higher-order shear deformation theory. Arch. Appl. Mech.. Appl. Mech. **93**(6), 2565–2583 (2023)
41. Chen, D., Gao, K., Yang, J., Kitipornchai, S.: An introduction to functionally graded porous materials and composite structures. In: Machine Learning Aided Analysis Design and Additive Manufacturing of Functionally Graded Porous Composite Structures, pp. 3–15. Elsevier (2024)
42. Chen, D., Yang, J., Kitipornchai, S.: Free and forced vibrations of shear deformable functionally graded porous beams. Int. J. Mech. Sci. **108**, 14–22 (2016)
43. Barati, M.R., Zenkour, A.M.: Investigating post-buckling of geometrically imperfect metal foam nanobeams with symmetric and asymmetric porosity distributions. Compos. Struct. **182**, 91–98 (2017)
44. Magnucki, K., Stasiewicz, P.: Elastic buckling of a porous beam. J. Theor. Appl. Mech. **42**(4), 859–868 (2004)
45. Chen, D., Yang, J., Kitipornchai, S.: Elastic buckling and static bending of shear deformable functionally graded porous beam. Compos. Struct. **133**, 54–61 (2015)
46. Gibson, I., Ashby, M.F.: The mechanics of three-dimensional cellular materials. Proc. Roy. Soc. Lond. A Math. Phys. Sci. **382**(1782), 43–59 (1982)

47. Choi, J., Lakes, R.: Analysis of elastic modulus of conventional foams and of re-entrant foam materials with a negative Poisson's ratio. Int. J. Mech. Sci. **37**(1), 51–59 (1995)
48. Detournay, E., Cheng, A.H.D.: 5-Fundamentals of poroelasticity. In: Fairhurst, C. (ed.) Analysis and Design Methods, pp. 113–171. Pergamon, Oxford (1993)
49. Reddy, J.N.: Energy Principles and Variational Methods in Applied Mechanics. Wiley, New York (2017)
50. Huang, Z., Lü, C., Chen, W.: Benchmark solutions for functionally graded thick plates resting on Winkler–Pasternak elastic foundations. Compos. Struct. **85**(2), 95–104 (2008)
51. Swaminathan, K., Naveenkumar, D.: Higher order refined computational models for the stability analysis of FGM plates—analytical solutions. Eur. J. Mech. A. Solids **47**, 349–361 (2014)
52. Rezaei, A., Saidi, A.: Application of carrera unified formulation to study the effect of porosity on natural frequencies of thick porous–cellular plates. Compos. B Eng. **91**, 361–370 (2016)
53. Thai, H.-T., Choi, D.-H.: An efficient and simple refined theory for buckling analysis of functionally graded plates. Appl. Math. Model. **36**(3), 1008–1022 (2012)
54. Ebrahimi, F., Habibi, S.: Deflection and vibration analysis of higher-order shear deformable compositionally graded porous plate. Steel Compos. Struct. **20**(1), 205–225 (2016)
55. Thai, H.-T., Choi, D.-H.: A refined plate theory for functionally graded plates resting on elastic foundation. Compos. Sci. Technol. **71**(16), 1850–1858 (2011)
56. Uymaz, B., Aydogdu, M.: Three dimensional mechanical buckling of FG plates with general boundary conditions. Compos. Struct. **96**, 174–193 (2013)
57. Uymaz, B., Aydogdu, M.: Three-dimensional vibration analyses of functionally graded plates under various boundary conditions. J. Reinf. Plast. Compos. **26**(18), 1847–1863 (2007)
58. Detournay, E., Cheng, A.H.-D.: Fundamentals of poroelasticity. In: Analysis and Design Methods, pp. 113–171. Elsevier (1993)
59. Ebrahimi, F., Habibi, S.: Deflection and vibration analysis of higher-order shear deformable compositionally graded porous plate. Steel Compos. Struct. **20**, 205–225 (2016)
60. Reddy, J.N.: Mechanics of Laminated Composite Plates and Shells: Theory and Analysis. CRC Press, London (2003)